

Comparison of Plasma Sheet and Auroral Electron Energy Fluxes During Substorms

M. O. Fillingim¹, G. K. Parks¹, R. P. Lin¹, and D. Chua²

¹Space Sciences Laboratory, University of California, Berkeley, CA 94720;
matt@ssl.berkeley.edu, parks@ssl.berkeley.edu, boblin@ssl.berkeley.edu

²Naval Research Laboratory, Washington, DC 20375;
dchua@ssd5.nrl.navy.mil

Abstract. Using both global auroral images and in-situ particle measurements, we quantitatively compare the downgoing electron energy flux in the plasma sheet with the electron energy flux into the auroral ionosphere with respect to substorm phase. We find that during quiet times, the downgoing energy flux in the plasma sheet mapped down to ionospheric altitudes is comparable to the energy flux observed in the aurora. During intervals of intense auroral emission such as substorm onset and expansion, the electron energy flux spectra in the conjugate region of the plasma sheet harden, increasing the downgoing energy flux. However, the increase in the plasma sheet energy flux is not enough to account for the increased energy flux into the ionosphere by up to an order of magnitude. This is consistent with the idea that additional energy flux is entering the loss cone through the presence of parallel electric fields above the ionosphere during intervals of intense auroral emission. As auroral activity decreases during recovery, the downgoing plasma sheet electron energy flux nearly sufficiently accounts for the diffuse auroral luminosity. Our results show that although large changes in the plasma sheet electron distributions occur at substorm onset, lower altitude processes are dominant in producing the observed auroral energy flux. These low altitude processes decrease in importance throughout the recovery phase.

1. Introduction

Recently there has been a renewed interest in the plasma sheet dynamics during times of active aurora such as substorms. Much of the work has emphasized the ion behavior [Angelopoulos *et al.*, 1997; Fairfield *et al.*, 1999; Fillingim *et al.*, 2000, 2001]. The electron behavior in the near-Earth plasma sheet during periods of auroral activity has largely been ignored. However, it is electron precipitation which is responsible for most of the observed auroral emission.

Here we investigate the adequacy of the near-Earth plasma sheet electron energy flux to power the aurora during quiet times, substorm expansion, and substorm recovery. We show results from two events during which we have favorable plasma sheet and auroral data: a quiet time pseudobreakup

and a substorm. We find that during quiet intervals and late in the substorm recovery, the downgoing electron energy flux in the plasma sheet is sufficient to power the observed aurora. During substorm onset and expansion, however, the precipitating electron energy flux into the auroral ionosphere can be up to an order of magnitude larger than the electron energy flux measured in the near-Earth plasma sheet.

These observations are consistent with the presence of a field aligned potential drop between the plasma sheet and the ionosphere which accelerates the particles and increases the precipitating electron energy flux during substorm onset and expansion. Assuming that a parallel electric field is responsible for contributing additional energy flux into the loss cone, we are able to estimate and monitor the total parallel

potential drop between the plasma sheet and the ionosphere throughout the phases of a substorm.

Also, we note that not all of the electron acceleration occurs at low altitudes in the auroral acceleration region. Simultaneous with auroral brightenings, a distinctive shift in the electron energy flux spectrum in the plasma sheet is observed which increases the downgoing electron energy flux by several hundred percent. These results indicate that although low altitude acceleration processes dominate during the initial phases of a substorm, other magnetospheric acceleration mechanisms are operating during substorm onset and throughout recovery which contribute to the auroral energy flux.

2. Observations

Our results are achieved by using global auroral images from POLAR/UVI [Torr *et al.*, 1995], from which we can derive the energy flux of the precipitating electrons, and the directly measured downgoing electron energy flux obtained by WIND/3DP [Lin *et al.*, 1995] in the near-Earth plasma sheet. Figure 1 shows three UVI images and three consecutive 3DP electron differential energy flux spectra which were observed during a pseudobreakup event on July 26, 1997.

The UVI images are shown in magnetic coordinates; local midnight is at the bottom. Each image was taken with a filter that passes the Lyman-Birge-Hopfield molecular nitrogen emissions in the wavelength range from 160 to 180 nm (LBH-long). The intensity of the auroral emission in this wavelength range is nearly directly proportional to the energy flux into ionosphere due to precipitating electrons [Germany *et al.*, 1997]. The integration time for each image was about 37 seconds. The time between successive images of the same filter and integration time was about three minutes. Due to the POLAR spacecraft “wobble,” the latitudinal extent of the region of intense auroral emission is exaggerated by 1.5 degrees at both the equatorward and poleward edges. The longitudinal extent is accurate to about one degree (about four minutes in local time). The ionospheric footprint of the WIND spacecraft calculated using the model of *Tsyganenko* [1989]

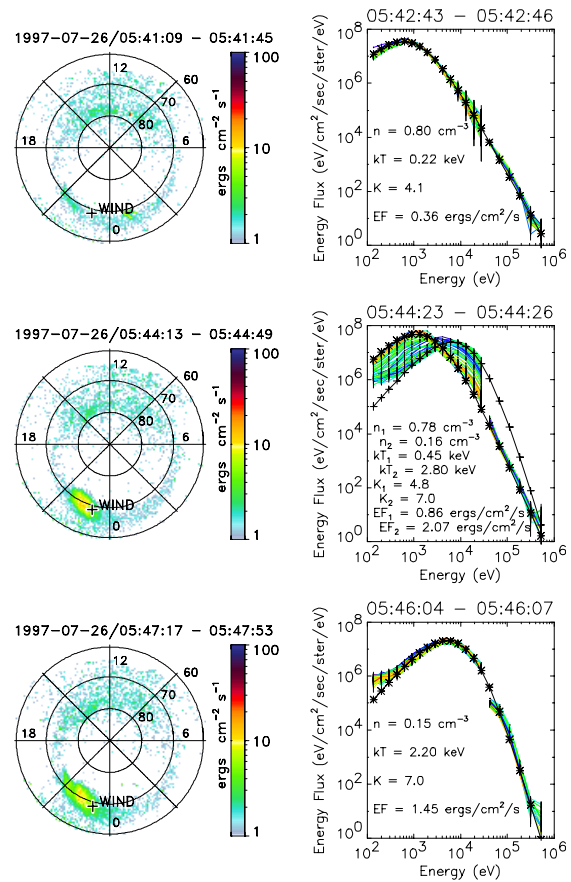


Figure 1. Three POLAR/UVI auroral energy flux images (left column) and three consecutive plasma sheet electron differential energy flux spectra measured by WIND/3DP (right column). The footprint of WIND is marked on each image.

is marked on each image. During this time, WIND was located at a GSM position of $[-11, 3, 0]$ R_E .

The electron energy flux spectra contain data from two detectors: the electron electrostatic analyzer (EESA), covering the energy range from 100 eV to 30 keV, and the solid-state telescopes (SST), covering energies from 30 keV to about 500 keV. The EESA data had an integration time of one spacecraft spin, about 3 seconds. In this mode of operation, the time between successive three-dimensional electron distributions was 1 minute 40 seconds. The SST data were integrated over 12 seconds, four spacecraft rotations, and were continuously collected. The SST data shown has the same start time as the EESA data. There are 88 individual curves in the EESA energy range, one

for each angular bin; likewise, there are 40 curves in the SST energy range. The curves are color coded according to pitch angle. Angular bins pointed in the field aligned direction are red. Bins pointed in the anti-field aligned direction are blue. Intermediate colors correspond to intermediate pitch angles. In each panel plotted along with the data is a kappa distribution whose parameters are based on the moments of the EESA distribution and the slope of the SST measurements. Also on each plot, the integrated electron energy flux is shown. This number is calculated by integrating the field aligned electron differential energy flux spectrum over energy from 100 eV to 500 MeV, multiplying the result by the solid angle of the loss cone, and mapping this quantity down to ionospheric altitudes.

The top row shows the aurora and electron data during quiet conditions. The auroral energy flux in the vicinity of the WIND footprint is near the UVI threshold of $1 \text{ erg/cm}^2/\text{s}$. In the plasma sheet, the downgoing electron energy flux mapped to the ionosphere was well under $1 \text{ erg/cm}^2/\text{s}$. However, since the auroral intensity is near the detectability limit of the UVI instrument, the uncertainty in the UVI measurement is large, and we are unable definitively say that there is a discrepancy between the two observations.

In the second row, the aurora has brightened significantly in the pre-midnight sector, though the region of intense auroral emission is localized. Since the exact footprint of WIND in the ionosphere is unknown, we take a box 1 hour in local time by 5 degrees in latitude, or approximately 1000 km by 1000 km, around the model derived footprint and calculate the median, minimum, and maximum energy flux values within this area to compare with those measured in the plasma sheet. The median energy flux into the ionosphere near the WIND footprint is about $3.5 \text{ ergs/cm}^2/\text{s}$; the minimum value is about 1 and the maximum value is over $10 \text{ ergs/cm}^2/\text{s}$.

The electron energy flux spectrum observed in the plasma sheet appears highly anisotropic. Close examination suggests that the electron distribution is time aliased, and that we are seeing the electron energy flux spectrum evolve from one similar to that in the top row to one like that seen in the third

row. (The SST data is not time aliased because its integration time spans several spacecraft rotations.) Choosing energy flux spectra from individual angular bins near the beginning and end of the integration time, we estimate the energy flux before and after the spectral change. The energy flux increases from $0.86 \text{ ergs/cm}^2/\text{s}$ to just over $2 \text{ ergs/cm}^2/\text{s}$, larger than a factor of 2. Both of these values are less than the median energy flux into the ionosphere determined from the UVI image; however, the larger value is slightly greater than the minimum energy flux seen near the WIND footprint.

In the third row, the electron precipitation continues, but the region of significant auroral emission remains localized. The energy flux values near the WIND footprint are between 1 and $8 \text{ ergs/cm}^2/\text{s}$ with the median value near $4 \text{ ergs/cm}^2/\text{s}$. The measured downward electron energy flux in the plasma sheet is around $1.5 \text{ ergs/cm}^2/\text{s}$. Again, the plasma sheet energy flux is less than the median ionospheric energy flux, but it is slightly larger than the minimum ionospheric energy flux.

Figure 2 shows ionospheric and plasma sheet electron energy flux data for a substorm on September 30, 1997, in a different format. The top panel shows the energy deposition rate (energy flux times area) into the ionosphere due to precipitating electrons as a function of latitude and time over a four hour interval. The horizontal black line marks the latitudinal position of the WIND footprint. The second panel similarly displays the magnetic local time extent of the energy deposition rate as a function time. The black line again shows the local time position of the WIND footprint. These two panels were constructed from consecutive 37-second LBH-long UVI images. During this interval UVI was operating in a mode such that there is one image every 37 seconds. It is clear that substorm onset precedes the first image at 03:53 UT. Due to unfavorable viewing geometry, no images are available before this time. There is a gap in the data apparent between 5:48 and 5:53 UT due to a change in the UVI platform viewing angle.

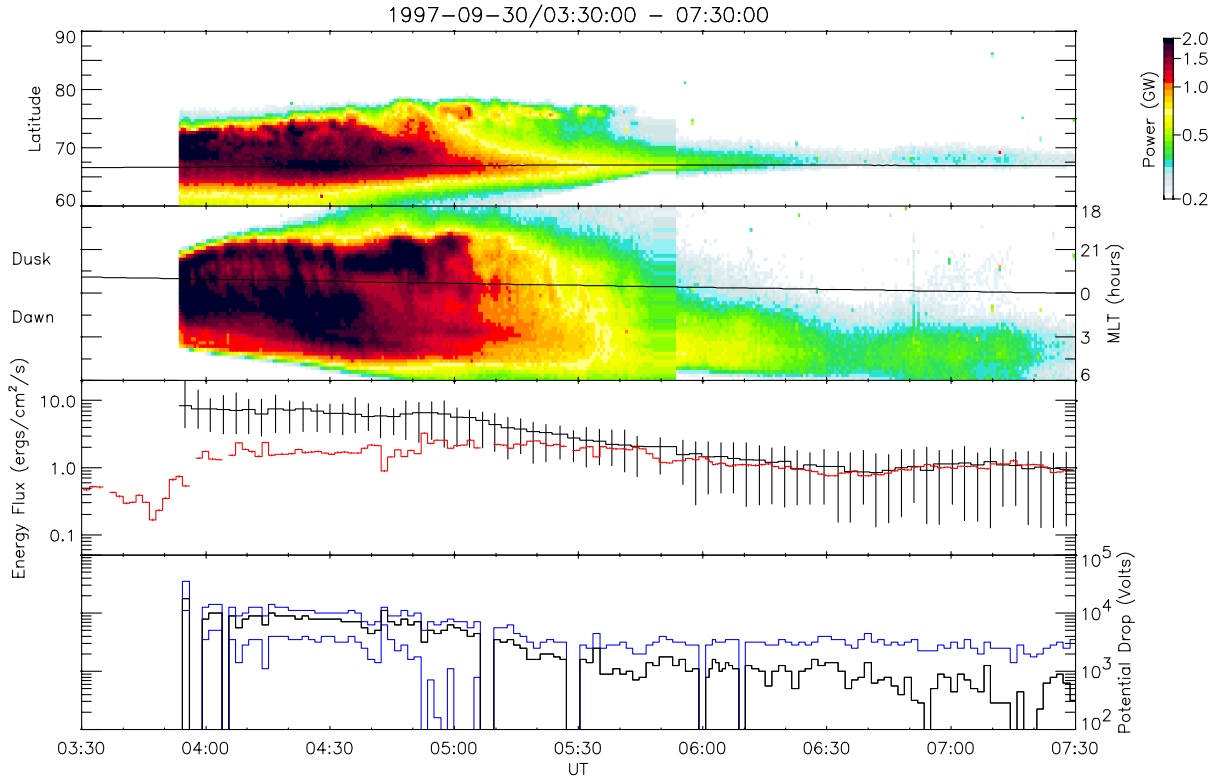


Figure 2. Comparison of auroral and plasma sheet electron energy fluxes. From top to bottom: auroral energy deposition rate (power) as a function of latitude and time; as a function of local time and time (with the WIND footprint marked in each panel); auroral energy flux near the WIND footprint (black) and downgoing plasma sheet electron energy flux mapped to ionospheric altitudes (red); total parallel potential drop between the plasma sheet and the ionosphere (blue curves are upper and lower estimates).

The electron energy flux into the ionosphere and in the plasma sheet is shown in the third panel. The top, black curve is the median ionospheric energy flux near the WIND footprint determined from the UVI images. The endpoints of the vertical lines represent the minimum and maximum energy flux values in the 1000 km by 1000 km area around the footprint. To prevent overcrowding, only the energy flux from every fifth image is plotted. The red curve shows the field aligned (downgoing) electron energy flux measured in the plasma sheet. Error bars based on Poisson counting statistics are plotted but are only slightly larger than the thickness of the energy flux curve.

Notice the large increases in the plasma sheet energy flux near 03:50 and again at 03:55 UT. Examination of the electron energy flux spectra at these times (not shown) reveals changes in the spectra similar to that seen in Figure 1. However,

even with these large increases in energy flux, it is clear that shortly after onset, once UVI starts imaging the aurora, even the minimum estimate of the ionospheric energy flux is much larger than the measured plasma sheet energy flux. Therefore, excess energy flux must be entering the loss cone.

One possible source of this excess energy flux is the presence of a field aligned electric potential drop between the plasma sheet and ionosphere. The bottom panel of Figure 2 plots the total potential drop between the plasma sheet and ionosphere based on this assumption. The middle, black curve shows the potential drop based on the median UVI energy flux. The upper and lower blue curves are based on the maximum and minimum ionospheric energy fluxes, respectively. The blue curves, then, indicate the upper and lower limits of the potential drop. The potential drop is calculated by shifting the observed field aligned plasma sheet

electron differential energy flux spectrum through a thin potential drop, integrating over energy and the loss cone solid angle, and mapping the integrated energy flux down to the ionosphere. The potential drop is chosen such that the difference between the observed ionospheric energy flux and the shifted plasma sheet energy flux is a few percent or less.

During substorm expansion, the parallel potential drop is on the order of 10 kV. As the substorm recovers, the estimated value of the potential drop gradually decreases. After 05:00 UT, the minimum value of the ionospheric energy flux falls below the plasma sheet energy flux, so the lower limit of the potential drop becomes 0 V. However, the median and maximum values of the ionospheric energy flux are still larger than those measured in the plasma sheet. After 06:00 UT the two energy flux values are in fairly good agreement, and the potential drop is estimated to be 1 kV or less. Using this method, we are able to estimate and remotely monitor the total potential drop between the plasma sheet and the ionosphere throughout an extended interval.

There are, however, several caveats and limitations to this method of which the reader should be made aware. The largest uncertainty is the magnetic mapping of the WIND footprint. The magnetic field model of *Tsyganenko* [1989] used here is a static model. Substorms almost by definition are dynamic. Rapid changes in the magnetic topology and field aligned currents affect where the footprint of WIND is in the ionosphere. As mentioned earlier, this is why we consider an area 1 hour in local time by 5 degrees in latitude (approximately 1000 km by 1000 km) around the modeled footprint when determining the ionospheric energy flux. This can lead to an uncertainty of up to an order of magnitude.

Such a large uncertainty prevents us from definitively stating whether the ionospheric and plasma sheet energy fluxes agree on July 26, 1997 (Figure 1). The median auroral energy flux is larger than the plasma sheet energy flux, but the minimum estimate of the auroral energy flux near the WIND footprint is less than the measured plasma sheet energy flux. However, shortly after onset on September 30, 1997, the discrepancy

between the auroral and plasma sheet energy fluxes is much larger than the uncertainty in the UVI energy flux estimates. In this case it is clear that an additional source of energy flux is needed, coming presumably from a field aligned potential drop.

Another limitation is that 3DP does not measure the loss cone distribution in the plasma sheet. At 11 RE near the equatorial plane, the loss cone is on the order of 1 degree. The angular resolution of the electron measurements is between 10 and 20 degrees, depending upon the look direction. We assume that the particle counts collected in the angular bin facing the field aligned direction are evenly distributed throughout that bin. If, for example, the loss cone were empty, we would be overestimating the downgoing plasma sheet electron energy flux. This, in turn, would lead to an underestimate of the total potential drop between the plasma sheet and ionosphere.

Additionally, there are limitations in the UVI image data. The UVI detection threshold is about 1 erg/cm²/s. For auroral energy fluxes less than this, counting statistics are poor and uncertainties are large. So if the UVI energy flux is near this lower limit and the plasma sheet energy flux less than 1 erg/cm²/s (as is the case for the top row of Figure 1), we are unable to state definitively if the two energy flux measurements agree or not.

Near apogee the resolution of UVI is about 30 km by 30 km. The energy flux from intense auroral features with scale sizes smaller than this (such as discrete auroral arcs) is spread out over the entire pixel area. As a result the peak energy flux determined from the auroral images may be considerably less than the actual peak energy flux in the ionosphere. In such a case, the values of the ionospheric energy flux and total potential drop would both be underestimated.

Similarly, the POLAR spacecraft wobble affects the UVI energy flux measurements. For small scale features, such as those shown in Figure 1, the wobble motion of the spacecraft smears out the image decreasing the auroral intensity (hence, energy flux) by up to a factor of 3. Again, the potential drop would likewise be underestimated. For large scale features, such as the substorm on

September 30, 1997 (Figure 2), this effect is not as important.

3. Summary and Conclusion

This paper has quantitatively compared the electron energy flux into the ionosphere responsible for the auroral emission to the downgoing electron energy flux measured in the conjugate region of the plasma sheet. Simultaneous with the onset of an auroral brightening, pseudobreakup or substorm, a distinctive change in the plasma sheet electron energy flux spectrum is observed. This spectrum change increases the downward electron energy flux incident on the ionosphere. However, the increased plasma sheet energy flux is not sufficient to produce the observed auroral intensity. Therefore, lower altitude processes must also play a role in accelerating the electrons and increasing the downgoing particle energy flux.

We are able to estimate the total parallel potential drop necessary to bring the ionospheric and plasma sheet energy fluxes into agreement. Fortuitous spacecraft placement allows for the remote monitoring of the total potential drop between the plasma sheet and ionosphere throughout the different phases of substorms. Using this method, we find that at substorm onset and expansion, the parallel potential drop can be on the order of 10 kV. During substorm recovery, the potential drop gradually decreases as the auroral intensity decreases. That is, lower altitude processes decrease in importance throughout substorm recovery.

Despite the large uncertainties and limitations associated with comparing the energy fluxes measured in the plasma sheet with those derived from auroral images, we are able to estimate parallel potential drops that compare favorably to those derived from low altitude particle measurements. This technique has the added advantage of being able to monitor the potential drop throughout the substorm sequence.

It is important to note that both high altitude (plasma sheet) and low altitude (auroral acceleration region) acceleration processes are operating during substorm onset, expansion, and

recovery. Answering the questions of what these different acceleration mechanisms are and how they interact will be the focus of future research.

Acknowledgments

WIND magnetometer data are courtesy of R. P. Lepping. This work was supported in part by NASA Grant Nos. NAG5-3170 and NAG5-26580.

References

- Angelopoulos, V., et al., Magnetotail flow bursts: association to global magnetospheric circulation, relationship to ionospheric activity and direct evidence for localization, *Geophys. Res. Lett.*, **24**, 2271-2274, 1997.
- Fairfield, D. H., et al., Earthward flow bursts in the inner magnetotail and their relation to auroral brightenings, AKR intensifications, geosynchronous particle injections and magnetic activity, *J. Geophys. Res.*, **104**, 355-370, 1999.
- Fillingim, M. O., et al., Coincident POLAR/UVI and WIND observations of pseudobreakups, *Geophys. Res. Lett.*, **27**, 1379-1382, 2000.
- Fillingim, M. O., et al., Comparison of plasma sheet dynamics during pseudobreakups and expansive aurora, *Phys. Plasmas*, **8**, 1127-1132, 2001.
- Germany, G. A., et al., Remote determination of auroral energy characteristics during substorm activity, *Geophys. Res. Lett.*, **24**, 995-998, 1997.
- Lepping, R. P., et al., The WIND magnetic field investigation, *Space Sci. Rev.*, **71**, 207-229, 1995.
- Lin, R. P., et al., A three-dimensional plasma and energetic particle investigation for the WIND spacecraft, *Space Sci. Rev.*, **71**, 125-153, 1995.
- Torr, M. R., et al., A far ultraviolet imager for the International Solar-Terrestrial Physics mission, *Space Sci. Rev.*, **71**, 329-383, 1995.
- Tsyganenko, N. A., A magnetospheric magnetic field model with a warped tail current sheet, *Planet. Space Sci.*, **37**, 5-20, 1989.